Sensors & Actuators: B. Chemical 418 (2024) 136231

Contents lists available at ScienceDirect

Sensors and Actuators: B. Chemical

journal homepage: www.elsevier.com/locate/snb

Amplification of photothermally induced reversible actuation in non-woven fabrics compared to bulk films

Michele Zanoni [a], Alessio Cremonini [a], Maurizio Toselli [b,c,d], Marco Montalti [a,c], Daniele Natali [b], Maria Letizia Focarete [a,c,e], Stefano Masiero [a], Chiara Gualandi [a,c,d,e,*]

[a] Department of Chemistry "Giacomo Ciamician", University of Bologna, Via Selmi 2, Bologna 40126, Italy
[b] Department of Industrial Chemistry "Toso Montanari", University of Bologna, Viale Risorgimento, 4, Bologna 40136, Italy
[c] INSTM UdR of Bologna, University of Bologna, Via Selmi 2, Bologna 40126, Italy
[d] Interdepartmental Center for Industrial Research on Advanced Applications in Mechanical Engineering and Materials Technology, CIRI-MAM, University of Bologna, Viale Risorgimento, 2, Bologna 40136, Italy
[e] Health Sciences & Technologies (HST) CIRI, University of Bologna, Via Tolara di Sopra 41/E, Ozzano Emilia Bologna 40064, Italy

ARTICLE INFO

Keywords:
Photoactuation
Two-way shape memory polymers
Azobenzene
Photothermal effect
Electrospinning

ABSTRACT

The burgeoning field of soft robotics has witnessed a surge in interest, driven by the pursuit of creating precise machines with soft actuators capable of surpassing or aiding human manufacturing capabilities. This work explores light-responsive shape memory actuators derived from electrospun fibers, integrating a "push-pull" azo compound into a poly(ε-caprolactone) matrix. Driven by photothermal conversion, the resulting system exhibits reversible actuation under UV light, demonstrating rapid responses and superior performance compared to film counterparts. More specifically, the significant impact of morphology on both the photothermal behavior and the actuation performance is highlighted by comparing non-woven and bulk shape memory material. The temperature variation induced by UV light in the non-woven was notably affected by scattering effects, leading to the formation of temperature gradients throughout the material. Notably, the study establishes a unique stress-responsive range for fibrous actuators, demonstrating that their porous structure contributes to higher actuation magnitudes at lower stresses compared to conventional films. This innovation holds promise for applications in micro-robotics and biomedical fields, showcasing the potential of fibrous actuators in augmenting human-friendly robotics through their lightweight, flexible, and remotely actuated features.

1. Introduction

The interest in soft robotics has experienced a continuous growth in recent years. Building soft actuators to develop precise machines that can overcome or assist human manufacturing ability represents a great challenge for the scientific community [1]. These actuators aim to become technological innovations fostering the development of human-friendly robotics. This involves, to some extent, replacing the rigid machines prevalent in contemporary industrial settings, sometimes characterized by limited adaptability and safety concerns. Among the countless applications of soft actuators, a notable function is the conversion of energy from one form to another. This encompasses the generation of mechanical energy through chemical processes, as well as the stimulation of artificial muscles through light activation [2]. In the field of soft robotics, artificial muscles are of particular interest due to their multiple applications in both mechanical and medical fields. In fact, they can replace various biological or mechanical components, executing reproducible processes with high energy conversion efficiency and without showing any deterioration. The realization of artificial muscles can be achieved through the use of shape memory polymers (SMPs), materials capable of retaining a temporary shape and subsequently reverting to their original form when exposed to an external stimulus such as magnetic field, moisture, light or heat [3]. The mode of action of a thermally-induced SMP is closely tied to polymer thermal transitions and it arises from the combination of the specific polymeric macromolecular architecture and the thermo-mechanical history of the sample [4].

Light constitutes a particularly attractive way for activating polymer actuators, owing to its easy spatial and temporal control, tunability and non-contact mode. In recent years, several examples of light-controlled

* Corresponding author at: Department of Chemistry "Giacomo Ciamician", University of Bologna, Via Selmi 2, Bologna 40126, Italy.
E-mail address: c.gualandi@unibo.it (C. Gualandi).

https://doi.org/10.1016/j.snb.2024.136231
Received 13 February 2024; Received in revised form 30 June 2024; Accepted 1 July 2024
Available online 9 July 2024

actuation [5–7] have been reported for polymeric materials, including hydrogels [8], liquid crystalline polymers and elastomers [9], and SMPs [10,11]. These materials rely on either photo-isomerizable moieties (e.g., azobenzene [12] and spirobenzopyran [13]) that undergo either a reversible photochemical reaction, generating tensional stress within the material (photomechanical effect), or a light-induced heating (photothermal effect) [14,15]. This last effect can be obtained also using photothermal additives (e.g., polydopamine (PDA) [16,17], polypyrrole [18], graphene [19] and graphene oxide [20], gold nanoparticles [21], and carbon nanotubes [22]) that convert photon energy into thermal energy (photothermal effect). Azobenzenes, in particular, are widely employed to achieve photothermal and photomechanical responses and have been selected as the "power unit" for various devices, including graspers [23–25], walkers [25,26], motors [27], and artificial muscles [28,29]. Azobenzenes can be reversibly photoisomerized from the more stable trans form to the cis form by irradiation with UV or visible light, depending on the nature of the substituents present. More exactly, irradiation of the trans isomer at a suitable wavelength produces a photostationary state, where there is a dynamic equilibrium between the two isomers. If the source of radiant energy is switched off, the equilibrium moves back to the trans form via thermal relaxation of the fraction of cis isomer present. In this case, the energy absorbed by the chromophore is released to the surrounding medium in the form of heat [30]. Alternatively, the cis isomer can be reverted to the trans form by irradiation at different -typically visible- wavelengths. The thermal relaxation time from the cis photostationary state is strongly influenced by the substitution pattern of the azo chromophore with cis lifetimes spanning from months down to fractions of milliseconds [31].

In recent years, the integration of specialized functionalities into textiles or garments has garnered significant attention within the realm of soft robotics and human-robot interfaces [32]. Fiber-based actuators have emerged as a prominent area of interest in this context. Drawing inspiration from biological muscles [33], fibrous actuators exhibit remarkable traits such as flexibility and pronounced anisotropic properties. Leveraging conventional textile processing techniques, fibers can be processed by twisting, weaving, and knitting, ultimately giving rise to both two-dimensional and three-dimensional configurations for yarns and textiles [34]. Electrospinning is a noteworthy innovative technology, capable of producing continuous fibers with submicrometric diameters. These fibers are typically collected in the form of non-woven structures, but they can also be ingeniously assembled to emulate the intricate architecture of biological tissues such as tendons and muscles [35,36]. Electrospun actuators that combine high surface area, porosity, flexibility, lightweight nature, and thermally triggered shape memory attributes have been the subject to comprehensive investigation [37]. However, limited efforts have been devoted to achieving remote actuation through the utilization of electromagnetic energy. In an intriguing study, a near-infrared laser was employed to remotely and reversibly actuate a PDA-coated electrospun liquid crystalline microfiber. This pioneering approach demonstrated rapid actuation with an impressive speed of approximately 1 s, facilitated by the microfiber's diameter [38]. The incorporation of PDA coating was also harnessed to induce one-way shape memory behavior in electrospun polyurethane [39]. Further complexity in remotely controlled geometry alterations was demonstrated through a dual-layer composite comprising electrospun fibers enriched with Fe_3O_4 nanoparticles and a thermoresponsive hydrogel [40].

With the aim to explore the performance and the potentialities of light-responsive actuators made of electrospun fibers, along with the possible benefits deriving from their non-woven structure, in this work, we used a system previously developed by our teams. This system, based on poly(ε-caprolactone) (PCL) crosslinked through a sol-gel reaction, exploits the low-temperature crystal-to-melt transition to achieve both one-way and two-way shape memory effects when subjected to a thermal stimulus [41,42]. The introduction of photo-responsiveness was accomplished by incorporating a "push-pull" azo compound, characterized by its rapid thermal reversion to the trans form (4.6 ms), promptly releasing heat upon exposure to UV irradiation [43]. This photothermal effect was exploited to create light-responsive actuators in the form of thin films and non-wovens made of microfibers. The photothermal behavior and the reversible actuation of these systems were comprehensively characterized, revealing notable performance distinctions attributed to their different morphologies. Specifically, the thermal response triggered by the UV light in the non-woven was significantly influenced by scattering effects, resulting in the establishment of temperature gradients across the material. Interestingly, under equivalent stress conditions, the porous structure demonstrated a greater actuation response compared to its film counterpart. This particular feature can be advantageous in scenarios where modest stresses must be sufficient to induce substantial alterations in geometry, as might be the case in micro-robotics and biomedical applications.

2. Results and discussion

2.1. Photoresponsive shape memory system

Our shape memory system is based on a α,ω-triethoxysilane-terminated poly(ε-caprolactone) (tPCL) network crosslinked through silica-based netpoints (Figs. 1a and 1c), which was explored by us in the past, both as thin films and electrospun mats. This system displays one-way and two-way shape memory behavior under a thermal trigger [44–47]. In this work, as a further advancement, the system was doped with an AZO-OH compound to confer photothermal responsiveness (chemical structure: Fig. 1a; electrospray ionization mass spectrum: Fig. S1; ^{1}H NMR spectrum: Fig. S2). Azobenzenes with short-lived cis isomers have been proposed as photothermal-driven photo-switches, where the heat released during the cis-trans isomerization fuels actuation [14,30,48]. The rate of cis-to-trans isomerization can be increased by push-pull electron-donating/withdrawing substituents in 4–4' position on the rings [43,49]. The AZO-OH compound selected for this work belongs to this category, exhibiting rapid thermal cis-to-trans isomerization not only in solution (isomerization mechanism: Fig. S3; UV-Vis spectrum: Fig. S4) but also in glassy and liquid-crystalline polymers [50].

The behaviour of the light-responsive shape memory actuators proposed in this work is schematically represented in Fig. 1. The AZO-OH concentration was set at 4 wt% for both film (labelled as tPCL-AZO-Film) and mat (labelled as tPCL-AZO-ES-CX) for comparison. Under UV irradiation (Fig. 1d), the heat released by the trans-cis-trans isomerization produces a local increase of the temperature of the polymer (Fig. 1e), inducing the melting of PCL crystal phase (Fig. 1f). At this stage, the sample, subjected to an increasing load, experiences a decrease in Young's modulus and reaches a certain deformation (ε^1_{ON}, Fig. 1g) which depends on the applied stress. By keeping the sample under a constant load, when the light is turned off, the temperature of the sample decreases and the polymer crystallizes under stress, leading to the well-known phenomenon of crystallization-induced elongation (CIE), reaching a higher value of strain ε^1_{OFF} (Fig. 1g). By switching on the UV lamp, the PCL crystal phase melts again, leading to the melting-induced contraction (MIC) of the sample [51–53]. This procedure can be repeated for many cycles (Fig. 1g) and the actuation reversibility depends on the stability of the crosslinking points which prevent chain creeping. The fast cis-to-trans isomerization of the AZO-OH compound allows a fast recovery of the initial trans state without the need to reconfigure the system with visible light, as instead necessary for other systems [54].

Fig. 2a-d reports representative Scanning Electron Microscopy (SEM) images of the electrospun fibers before (sample tPCL-AZO-ES) and after the crosslinking treatment (sample tPCL-AZO-ES-CX). It was previously demonstrated that the same polymeric system, without the AZO-OH additive, is partially crosslinked after the electrospinning process but requires a thermal treatment to furtherly promote crosslinking and

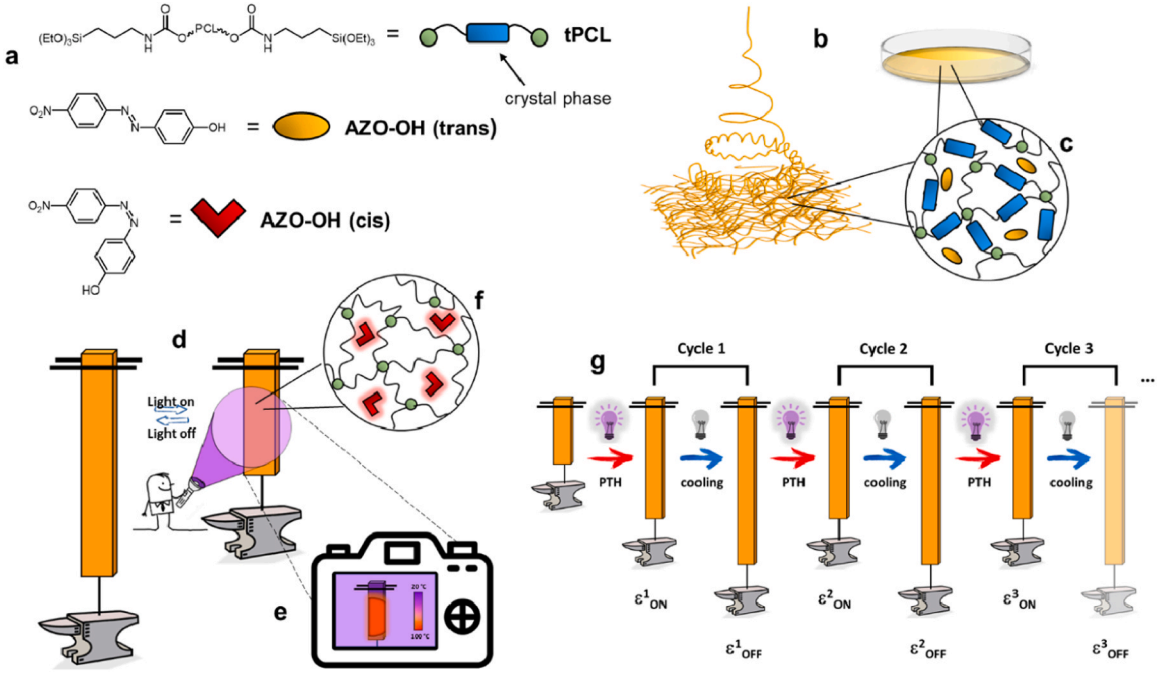

Fig. 1. Sketch describing the photo-activated two-way shape memory system: chemical structures of tPCL and AZO-OH (trans and cis forms) (a) used to produce non-woven mats (by electrospinning) and thin films (by solvent-casting) (b); the resulting materials consist of a network of chemically crosslinked semicrystalline PCL chains doped with 4 wt% of AZO-OH (c); both systems are tested under a constant load for two-way shape memory behavior using UV irradiation (d) while measuring the temperature of the sample with a thermal camera (e); UV light induces trans-to-cis isomerization of the dispersed AZO-OH, whose cis form spontaneously reverts to the trans one releasing heat, with the consequent melting of PCL crystal phase (photothermal heating, PTH) (f); both systems are tested up to 10 cycles by applying different pre-stretch strains, ε^1_{ON} (g).

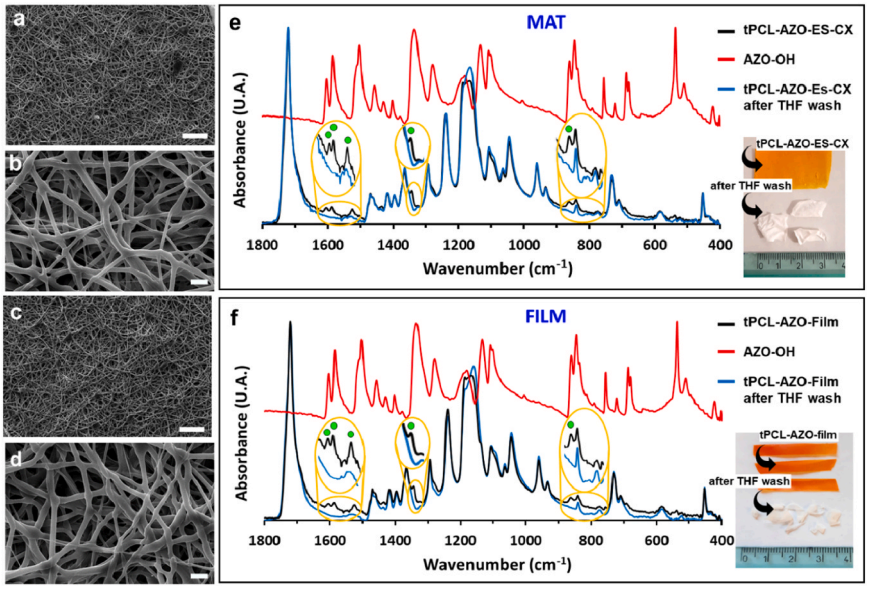

Fig. 2. Representative SEM images of tPCL-AZO-ES (a, b) and tPCL-AZO-ES-CX (c, d). e) ATR-IR spectroscopy of tPCL-AZO-ES-CX (black), the same sample after THF immersion (blue), and AZO-OH compound (red); pictures of tPCL-AZO-ES-CX before and after THF immersion are reported on the right. f) ATR-IR spectroscopy of tPCL-AZO-Film (black), the same sample after THF immersion (blue), and AZO-OH compound (red); pictures of tPCL-AZO-Film before and after THF immersion for 10 min are reported on the right. Scale bar = 100 μm (a and c); 10 μm (b and d).

improve the density of netpoints [45]. The average fiber diameter (Fig. S5) does not significantly change after the crosslinking treatment and it is in the 2–3 μm range. Both electrospun mats and films show an intense yellow color (see pictures in Fig. 2e and f) given by the AZO-OH doping. The presence of the AZO-OH compound in the samples is also confirmed by Attenuated Total Reflection Infrared (ATR-IR) spectroscopy. Indeed, the IR peaks characteristic of AZO-OH are clearly visible in both tPCL-AZO-ES-CX and tPCL-AZO-Film (C-N stretching at 1605 cm^{-1}; aromatic C-C stretching at 1588 cm^{-1}; N-O asymmetric and symmetric stretching at 1516 and 1331 cm^{-1}, respectively; out-of-plane bending of aromatic C-H at 863 and 845 cm^{-1}), together with the peaks assigned to PCL (C═O stretching at 1723 cm^{-1}; C-O-C asymmetric and symmetric stretching at 1240 and 1162 cm^{-1}, respectively). The AZO-OH compound is not covalently linked to the polymeric network,

being easily washed away when the samples are immersed in tetrahydrofuran (THF) (see the loss of yellow color in pictures of Fig. 2e and f and the disappearance of the AZO-OH infrared peaks in tPCL-AZO-ES-CX and tPCL-AZO-Film washed in THF).

As a general consideration, in two-way shape memory systems, the actuation magnitude ($\mathbf{R_{act}} = \varepsilon^{N}_{OFF} - \varepsilon^{N}_{ON}$, Equation 1 in the Supplementary Material) is governed by the amount of crystal phase (Fig. S6 shows that film and non-woven have the same X-ray diffraction pattern) that melts and crystallizes in the MIC and in the CIE stages, respectively. The crystallinity degree, in turn, depends on the crosslinking density, since the presence of netpoints can limit the structural arrangement of chains in an ordered structure [55,56]. Moreover, the crosslinking degree also affects the amorphous chain extension during CIE, imposing constraints against deformation, thus having an impact on the actuation. On the other hand, enough netpoints are a prerequisite to avoid undesired long-range molecular chains slippage and creep above polymer melting temperature [51]. For our systems, the effectiveness of the crosslinking procedure and the resulting thermal properties were verified by Differential Scanning Calorimetry (DSC) and gel content measures. Fig. 3 reports the DSC curves of tPCL-AZO-ES-CX and tPCL-AZO-Film, together with tPCL-AZO-ES to assess the effect of post-crosslinking on the fibers. For each sample, the calorimetric data are reported in Table 1. Data related to the first heating scans are highly dependent on the different thermal histories of the samples and therefore are not considered. Instead, the second heating scans allow a more reliable comparison between the samples and better represent the thermal behaviour of the actuators since, before applying the pre-stretching, their thermal history is erased by melting above T_m. In the second heating scan, the melting enthalpy of tPCL-AZO-ES (ΔH_m = 63 J g^{-1}) decreases after post-crosslinking (ΔH_m = 51 J g^{-1}), resulting in the reduction of the crystallinity, showing a value similar to that of the film (ΔH_m = 54 J g^{-1}). This trend confirms the effectiveness of the post-crosslinking in enhancing the netpoint density in the fiber. Similar results are obtained when comparing the undoped samples, i.e. tPCL-ES and crosslinked tPCL-ES-CX (Fig. S7 and Table S1). In Fig. 3, it is highlighted that the melting phenomenon for both crosslinked mat and film ends at 55 °C in the 2nd heating scan (T_m^{end}, dashed black line). This

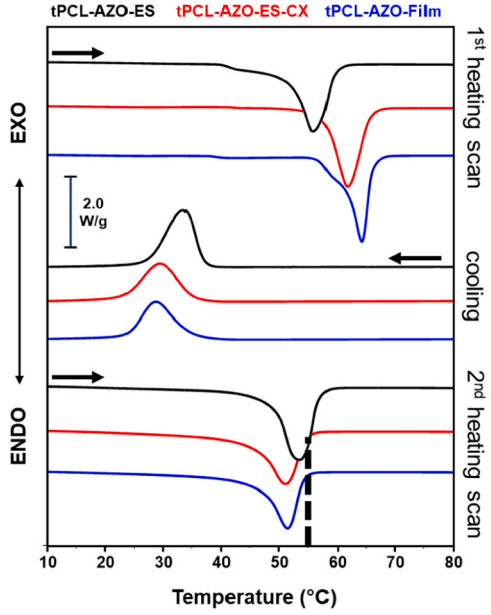

Fig. 3. DSC 1st heating scans (top), cooling scans (middle), and 2nd heating scans (bottom) of tPCL-AZO-ES (black), tPCL-AZO-ES-CX (red) and tPCL-AZO-Film (blue). The dashed black line crossing the 2nd heating scans indicates the end of the melting phenomenon for crosslinked mat and film (red and blue curves, respectively), T_m^{end} = 55°C.

will be a key aspect in the following discussion related to the photothermal effect. The gel content, namely the insoluble portion of the sample, was in the range of 88–95 % for both systems. Being both gel content and melting enthalpy of the crosslinked film and mat similar, a direct comparison of actuation performance of the two systems is feasible.

2.2. Photothermal behaviour

In shape memory materials activated by the photothermal effect, the intensity of the radiation is another parameter that can heavily affect the actuation since it controls the sample temperature [14]. The photothermal effect promoted by the AZO-OH on crosslinked PCL film and mat has been assessed at different radiation intensities by changing the distance of the UV lamp from the samples (Fig. S8a shows the correlation between light intensity and distance). A thermal camera was used to measure the temperature of the specimen, both on the side directly illuminated by the lamp (front) and on the opposite one (back). For both film and mat, when the lamp is turned on, the temperature of the two surfaces immediately rises, reaching a plateau value after about 15 and 10 s on the front and back sides, respectively, albeit at the highest distances it takes a bit more time for the temperature to stabilize over a constant value (Fig. S9). As expected, the closer the sample is to the UV source, the higher the temperature. When the light is turned off, the temperature rapidly decreases. Fig. 4a and b report the plateau temperatures measured on the front and back sides of both mat and film as a function of light intensity and distance from the UV source, respectively. The temperature is linearly correlated with the light intensity and the value measured on the side under direct irradiation is significantly higher than that on the back side. Interestingly, the temperature gradient across sample thickness is remarkably higher in the mat than in the film. Moreover, when placed at the same distance from the lamp, the temperature of the irradiated side of the mat is higher than that of the film. These results are somehow counterintuitive, as one would expect, by comparing mat and film, that the mat should display a lower temperature at the front side as a consequence of its higher porosity and, hence, of a lower AZO-OH density per unit volume. Moreover, for the same reason, a lower temperature gradient may be expected in the mat. These opposite results can be rationalized by considering the optical behaviour of electrospun mats, known to be highly reflective thanks to their ability to scatter light [58,59]. Light scattering at fiber surface is the consequence of the different refractive indices of air and fiber and results in the reduction of transmitted light through the mat and in multiple absorptions at fiber surface. Multiple absorptions of reflected UV light can thus justify the higher temperature recorded at the front surface of the mat compared to the film. The higher temperature gradient recorded for the mat can instead be explained by the low thermal diffusivity of the air entrapped between mat pores, which contributes to thermally isolating the cold back side of the mat from the hot front side.

The most important consequence of the photothermal effect is the melting of PCL crystal phase and, consequently, the change of sample mechanical properties. Fig. 4d-e shows the tensile stress-strain curves respectively of the mat and the film UV-irradiated by positioning the lamp at different distances from the sample (Fig. 4c). It is evident that both samples experience a large decrease in Young's modulus and strength under UV light. Interestingly, the mat displays a progressive reduction of mechanical properties by decreasing lamp distance from 6 to 5 cm, while from 4 cm onwards the stress-strain curves are overlapped. Differently, the maximum reduction of film mechanical properties occurs already at 6 cm and the decrease of lamp distance does not contribute to further reducing the mechanical properties. This is evident by considering how the Young's modulus of film and mat changes as a function of light intensity and lamp distance (Fig. 4f and g, respectively). This different trend of the elastic moduli is ascribable to the above-explained photothermal behavior and can be correlated to the average

Table 1
Relevant calorimetric data of tPCL-AZO electrospun samples (before and after the post-crosslinking) and film.

Sample	*1st heating scan*			*cooling*		*2nd heating scan*			
	T_g [°C]	T_m [°C]	ΔH_m [J g^{-1}]	T_c [°C]	ΔH_c [J g^{-1}]	T_g [°C]	T_m [°C]	ΔH_m [J g^{-1}]	X_c^a [%]
tPCL-AZO-ES	-51	56	85	33	63	-54	54	63	48
tPCL-AZO-ES-CX	-51	62	72	28	51	-53	51	51	39
tPCL-AZO-Film	-54	64	73	29	51	-51	51	54	39

a) calculated as $X_c = \frac{\Delta H_m}{f_w^{tPCL} \Delta H_m^0} \times 100$, where ΔH_m^0 is the melting enthalpy of the 100 % crystalline PCL (139.5 J g^{-1}) [57] and f_w^{tPCL} is the weight fraction of tPCL (0.96).

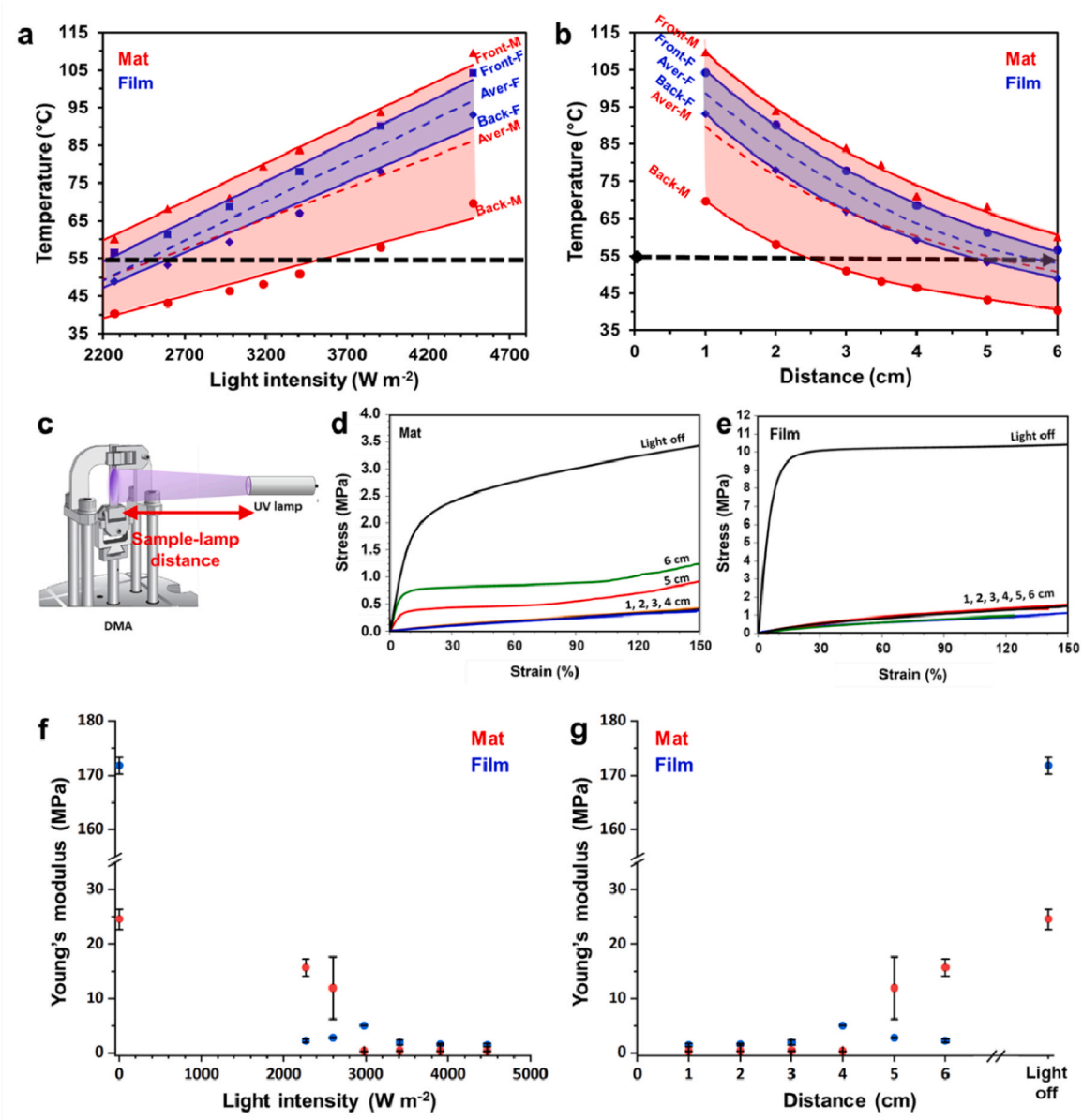

Fig. 4. Temperature as a function of light intensity (a) and temperature as a function of lamp distance (b) of tPCL-AZO-ES-CX electrospun mat (red) and of tPCL-AZO-Film (blue) measured by the thermal camera on both the front and back side of UV-irradiated samples; red and blue dashed lines represent the average temperature (T_{aver}) at each irradiating condition, black dashed line marks the T_m^{end} of PCL melting. Sketch showing the UV lamp positioned at different distances from the sample (c) and corresponding stress-strain curves of electrospun mat tPCL-AZO-ES-CX (d) and film tPCL-AZO-Film (e). Young's moduli (n=3) of UV-irradiated samples of tPCL-AZO-ES-CX electrospun mat (red) and tPCL-AZO-Film (blue) as a function of light intensity (f) and as a function of lamp distance (g).

temperature (T_{aver}) reached by the samples irradiated at different distances (Fig. 4b, dashed curves). The T_{aver} of the film is always higher than 55 °C (T_m^{end} of PCL melting), while the T_{aver} of the mat is higher than 55 °C only at distances lower than 4 cm. In other words, at distances higher than 4 cm the PCL crystal phase in the fibers is not entirely melted.

2.3. Shape memory behavior

The data related to the photothermal effect allowed us to properly set up the experimental conditions for actuation experiments. The more critical parameter is the distance between the sample and the UV source as it determines both the light intensity (Fig. S8a), thus the sample temperature, and the light spot size, thus the portion of the sample that can effectively be photo-activated (Fig. S8b). In order to maximize the spot size and to ensure the complete melting of PCL crystal phase in both film and mat, the actuation experiments were carried out by positioning the UV lamp at 3.5 cm from the samples (ca. 3000 W m^{-2}).

Actuation experiments were carried out by subjecting the samples to different levels of pre-stretch (ε^1_{ON}) and by monitoring the strain during subsequent UV-on/UV-off cycles, over 10 cycles, for both mat and film (Fig. 5a-b). For all samples, a reversible strain elongation/ contraction can be observed. In the time interval of each cycle (30 s UV on + 30 s UV off), the materials display a fast shape change (c.a. 10 s), both during contraction and elongation. For a better quantification of the shape memory behavior, the actuation magnitude (R_{act}), namely the net elongation induced by cooling, and the actuation reversibility (R_{rec}), namely the percentage of cooling-induced elongation recovered by heating, are reported for each cycle in the Supplementary Material (Table S2, Table S3 and Fig. S10). The data show that the film displays a good recovery of the shape in the first cycle of each condition of actuation, with R_{rec} higher than 95 %, approaching 100 % in the subsequent cycles. For similar pre-stretch, the fibrous mat generally shows lower R_{rec} in the first cycles, with values that span from 95 % at low pre-stretch to 73 % at high pre-stretch. Moreover, incomplete recovery can also persist in the second cycle for electrospun material when subjected to the highest deformations. Similar results were previously found under thermal actuation [44] and were ascribed to the probable microstructural modification of the mat occurring when high pre-stretches are applied (>100 %). Under this condition, mutual sliding and rearrangements of the fibers determine a partial recovery in the first cycles and give rise to a new fiber arrangement that becomes the reference state for the subsequent cycles. After the third cycle, both mat and film show values of R_{rec} close to 100 % and constant R_{act}, thus approaching a stable behavior (Table S2 and S3). The thermo-mechanical and shape memory properties of both film and electrospun mats loaded with AZO-OH agree with those described previously for the same crosslinked PCL (without azo) directly thermally activated, except for a faster change of the shape when the thermal stimulus is photo-induced (Fig. S11) [42,44,47].

To facilitate the comparison between the two systems, Fig. 6a and 6b show R_{act} and R_{rec} calculated as the average from cycle 3 to cycle 10 as a function of pre-stretching (data reported in Table 2). No relevant differences emerge when comparing the behaviour of the mat and the film, demonstrating that the actuation amplitude depends on the pre-stretching and it is not affected by the sample morphology. Indeed, as expected, it increases with pre-stretching for both materials up to 100 % of ε^1_{ON} reaching a plateau in the range 60–70 % for the film and 50–60 % for the mat. The actuation recovery is always close to 100 % (Fig. 6b).

Noticeable differences in the behaviour of mat and film become apparent when plotting the actuation amplitude as a function of the applied stress (Fig. 6c). The plot clearly highlights that the mat and the film operate in distinct and non-overlapping stress ranges. Specifically, the mat operates within a stress range of 0.15–0.40 MPa, similar to human muscle [60,61], while the film operates between 0.4 and 1.1 MPa. In other words, the electrospun mat is pre-stretched and can actuate similarly to the bulk film but under lower levels of applied stresses. The reason why the mat response can be triggered by lower stress compared to the corresponding films lies in the lower densities featured by the former. The difference in actuation performance is further highlighted when we compare film and non-woven working under similar loadings (Table S4), in terms of work capacity (130 J Kg^{-1} and 340 J Kg^{-1}, respectively) and actuation rate (5.8 % $s^{-1}$and 10.5 % s^{-1}, respectively). A further indication of the improved performance of non-woven comes out by plotting the R_{act} as a function of the number of times the materials can lift their own weight (Fig. 6d). This measurement is somewhat debatable because the weight lifted by the sample depends on the sample cross-section, while the weight of the specimen depends on its density and dimension. This means that to minimize the weight of the sample, one could simply reduce its length. However, the "times its own weight" parameter is frequently used to emphasize how much these polymer actuators are lightweight compared to the weights they can lift [17,62,63]. In our case, we considered mats and films of comparable length and we determined the number of times the material

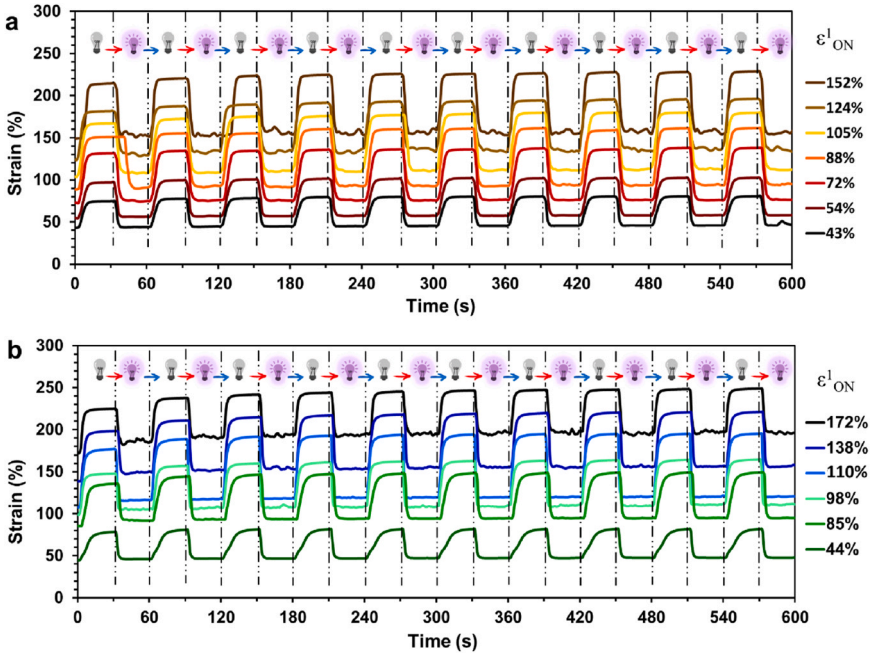

Fig. 5. Actuation experiments carried out on tPCL-AZO-Film (a) and on tPCL-AZO-ES-CX electrospun mat (b) by applying different stresses to achieve different values of pre-stretch (ε^1_{ON}). In each experiment, the stress was kept constant while the UV lamp was alternatively turned on and off every 30 s, to complete 10 cycles.

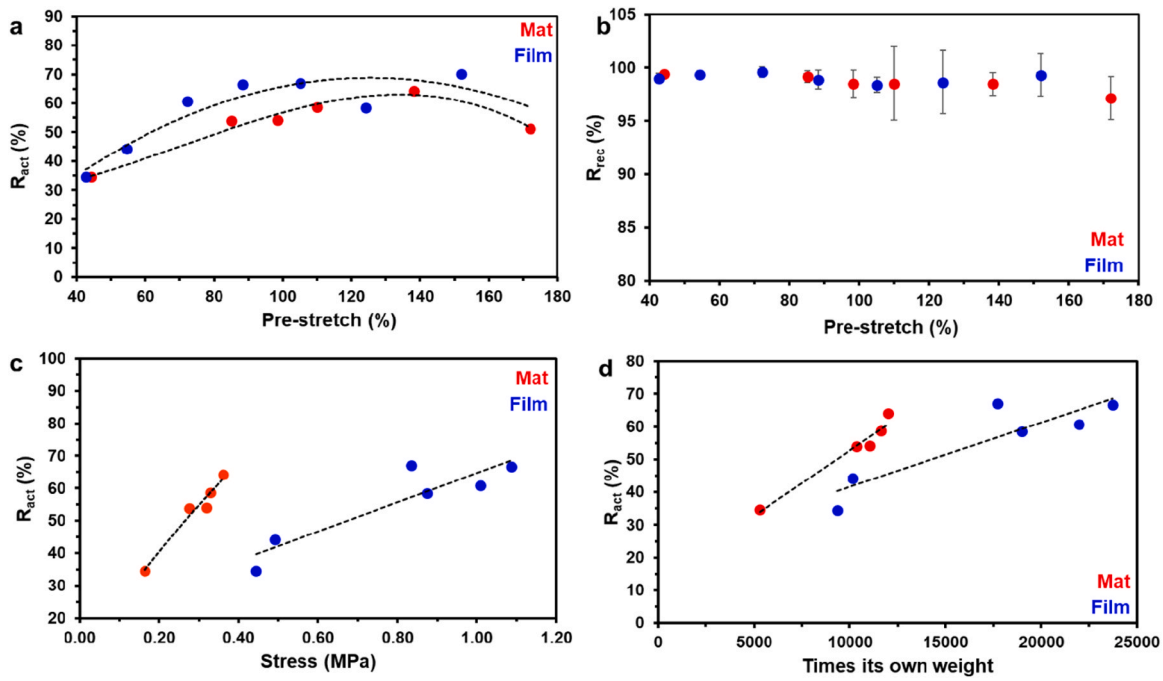

Fig. 6. Comparison of two-way shape memory behavior of tPCL-AZO-Film and tPCL-AZO-ES-CX electrospun mat: a) actuation magnitude as a function of the pre-stretch (ε^1_{ON}); b) actuation recovery as a function of the pre-stretch (ε^1_{ON}), as average values from cycle 3 to cycle 10 (±SD); c) actuation magnitude as a function of the applied stress; d) actuation magnitude as a function of the number of times the material can lift its own weight.

Table 2
Results of the two-way shape memory response for tPCL-AZO-Film and tPCL-AZO-ES-CX subjected to various initial pre-stretch (ε^1_{ON}) and stress conditions.

Sample	ε^1_{ON} [%]	Stress [MPa]	R_{act} [a] [%]	R_{rec} [b] [%]
tPCL-AZO-Film	43	0.44	35.6 (0.4)	99.4 (0.3)
	54	0.49	44.3 (0.3)	99.7 (0.5)
	72	1.01	61 (1)	99.8 (0.7)
	88	1.09	67 (2)	99 (1)
	105	0.84	67 (1)	99 (1)
	124	0.88	58 (2)	99 (3)
	152	1.49	70 (1)	99 (3)
tPCL-AZO-ES-CX	44	0.16	34.6 (0.1)	99.7 (0.2)
	85	0.28	53.9 (0.3)	99.6 (0.5)
	98	0.32	54.1 (0.7)	99 (1)
	110	0.33	59 (1)	99 (2)
	138	0.36	64.2 (0.8)	99 (2)
	172	0.48	51.3 (0.8)	99 (3)

[a] calculated by applying Equation 1, expressed as average values from cycle 3 to cycle 10 ± SD (in brackets);
[b] calculated by applying Equation 2, expressed as average values from cycle 3 to cycle 10 ± SD (in brackets).

can lift its own weight (Fig. 6d) as described in the Supplementary Material (Table S5 and S6). Fig. 6d shows the rise of the actuation magnitude with the increase of applied weight for both samples, as expected. The plot confirms the different ranges of lifted weight and, more importantly, it reveals that, by keeping the number of times of the lifted weight constant, the actuation magnitude is higher for the mat compared to the film. In other words, the mat better amplified the stress applied, generating a higher actuation. It is also pointed out that the number of times the material can lift its weight reported in Fig. 6d is not the maximum one; thus, higher weights can be sustained without breaking the samples. However, in these cases, the actuation magnitude did not increase further.

This outcome can have direct and intriguing implications in various applications where small stresses can be leveraged to generate substantial and reversible deformations. As a proof of concept, a small home-built lever can be used to harness the force generated by the suspended weight to pre-stretch the sample (Fig. 7, Video S1 and S2). Upon exposure to UV light, the sample undergoes melt-induced contraction, causing the lever to move and lift the weight reversibly. In this particular example, both the tested mat and film have identical dimensions (20 mm length, 5 mm width, and 0.1 mm thickness), and the weight applied is approximately 2.5 g. Under these specific conditions, upon UV illumination, the mat lifts the weight by about 5 cm, whereas the corresponding film only lifts it by 3.5 cm.

As a final comparison, we tested the durability of these systems over hundreds of cycles. Specifically, both the film and non-woven materials were pre-stretched to approximately 80 % deformation and photo-actuated for 6 h under repeated UV-ON/UV-OFF cycles, up to 360 cycles. Under these conditions, R_{act} did not significantly change in both materials. However, the film failed after 315 cycles, whereas the non-woven material endured until the end of the experiment (Fig. S12). In another experiment to assess the durability and resistance of the materials under prolonged UV exposure, both the film and non-woven were cycled 10 times and subsequently exposed to continuous UV light for 30 min at rest. After this treatment, the film failed during the pre-stretching step, while the non-woven successfully completed an additional 10 cycles. The non-woven was further exposed to UV light for an additional 30 min, reaching a cumulative exposure of 120 min, and was re-cycled every 30 min for 10 cycles without any significant deterioration in photoactuation performance (Fig. S13). Overall, non-woven mats outperform the corresponding bulk materials, both in terms of actuation performance and durability. The good performance of the proposed non-woven system comes out also when comparing its actuation magnitude, work capacity, response time and weight lifted with those reported by other soft actuators based on photoactivated shape memory polymers (Table S7).

3. Conclusion

Light-responsive actuators, specifically based on electrospun fibers, have been explored in this study. The overarching goal was to investigate the potential benefits of non-woven structures in comparison to

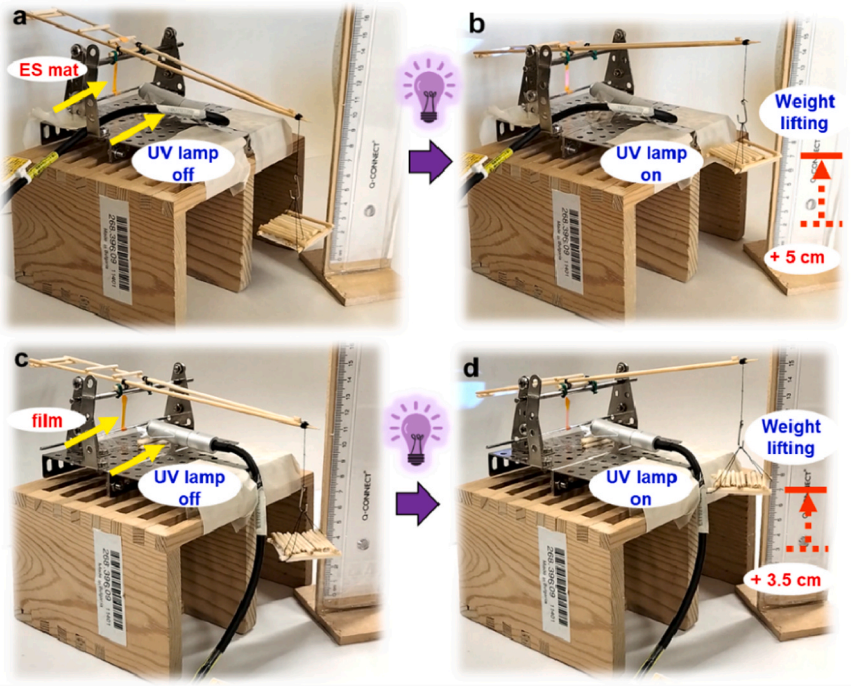

Fig. 7. tPCL-AZO-ES-CX mat (a and b) and tPCL-AZO-Film (c and d) are mounted on a custom-made lever with a counterweight of 2.5 g. The UV light source is positioned in front of the sample at a distance of 3.5 cm. When the light is turned on the samples experience a melt-induce contraction, leading to the movement of the lever and the lifting of the counterweight: the mat raises the weight by 5 cm (b) while the film lifts it by 3.5 cm (d). Pictures are frames selected from Supplementary Video S1 and S2.

traditional film configurations. The study focused on a shape memory system based on poly(ε-caprolactone) (PCL) crosslinked through a sol-gel reaction, incorporating a "push-pull" azo compound for photo-responsiveness. The photothermal effect induced by the azo compound led to the melting of the PCL crystal phase, resulting in reversible shape changes. Detailed analyses, including SEM images, ATR-IR spectroscopy, and DSC measurements, provided insights into the structural and thermal characteristics of the electrospun fibers. The study systematically explored the influence of radiation intensity, distance from the UV source, and sample morphology on the temperature distribution and mechanical properties during actuation. Actuation experiments revealed that both the electrospun mat and film exhibited reversible strain elongation/contraction. The actuation amplitude was found to depend on the pre-stretching level, with both mat and film displaying similar trends. Notably, the comparison between the electrospun mat and film highlighted distinct stress ranges of operation. The mat exhibited an actuation response within a stress range comparable to human muscle, emphasizing its potential in applications where lower stresses can be leveraged to achieve significant deformations. This unique characteristic was further highlighted in a practical demonstration using a home-built lever, showcasing the mat's ability to generate higher actuation magnitudes compared to the film under the same applied weight. Overall, this research contributes valuable insights into the design and optimization of light-responsive actuators based on electrospun fibers, paving the way for their application in diverse fields, including soft robotics and biomedical devices. The study underscores the importance of considering morphology and material composition in tailoring the performance of shape memory systems for specific applications. Future work in this area may explore additional functionalizations, scalability, and practical implementations in real-world scenarios.

CRediT authorship contribution statement

Marco Montalti: Writing – review & editing, Conceptualization. **Daniele Natali:** Investigation. **Maria Letizia Focarete:** Writing – review & editing, Funding acquisition. **Michele Zanoni:** Methodology, Investigation, Conceptualization. **Alessio Cremonini:** Investigation. **Maurizio Toselli:** Writing – review & editing, Conceptualization. **Stefano Masiero:** Writing – original draft, Supervision, Conceptualization. **Chiara Gualandi:** Writing – original draft, Supervision, Project administration, Funding acquisition, Conceptualization.

Declaration of Competing Interest

The authors declare that they have no known competing financial interests or personal relationships that could have appeared to influence the work reported in this paper.

Data availability

Data will be made available on request.

Acknowledgement

The work has been funded by the European Union - NextGenerationEU under the National Recovery and Resilience Plan (PNRR) - Mission 4 Education and research - Component 2 From research to business - Investment 1.1 Notice Prin 2022 - DD N. 104 del 02/02/2022, from the project "ALICE - light-Activated high-performance actuators by electrospinning of reversibly crosslinked LIquid CrystallinE networks", proposal code 20224EBZ3Y – CUP J53D23008450006.

Appendix A. Supporting information

Supplementary data associated with this article can be found in the online version at doi:10.1016/j.snb.2024.136231.

References

[1] F. Schmitt, O. Piccin, L. Barbé, B. Bayle, Soft robots manufacturing: a review, Front. Robot AI 5 (2018), https://doi.org/10.3389/frobt.2018.00084.

[2] H. Koerner, T.J. White, N.V. Tabiryan, T.J. Bunning, R.A. Vaia, Photogenerating work from polymers, Mater. Today 11 (2008) 34–42, https://doi.org/10.1016/S1369-7021(08)70147-0.

[3] Y. Xia, Y. He, F. Zhang, Y. Liu, J. Leng, A review of shape memory polymers and composites: mechanisms, materials, and applications, Adv. Mater. 33 (2021) 2000713, https://doi.org/10.1002/adma.202000713.

[4] G. Scalet, Two-way and multiple-way shape memory polymers for soft robotics: an overview, Actuators 9 (2020) 10, https://doi.org/10.3390/act9010010.

[5] S. Nocentini, C. Parmeggiani, D. Martella, D.S. Wiersma, Optically driven soft micro robotics, Adv. Opt. Mater. 4 (2018) 1800207, https://doi.org/10.1002/adom.201800207.

[6] G. Stoychev, A. Kirillova, L. Ionov, Light-responsive shape-changing polymers, Adv. Opt. Mater. 7 (2019) 1900067, https://doi.org/10.1002/adom.201900067.

[7] M.R.A. Bhatti, A. Kernin, M. Tausif, H. Zhang, D. Papageorgiou, E. Bilotti, T. Peijs, C.W.M. Bastiaansen, Light-driven actuation in synthetic polymers: a review from fundamental concepts to applications, Adv. Opt. Mater. 10 (2022) 2102186, https://doi.org/10.1002/adom.202102186.

[8] L. Li, J.M. Scheiger, P.A. Levkin, Design and applications of photoresponsive hydrogels, Adv. Mater. 31 (2019) 1807333, https://doi.org/10.1002/adma.201807333.

[9] T.J. White, Photomechanical effects in liquid crystalline polymer networks and elastomers, J. Polym. Sci. B Polym. Phys. 56 (2018) 695–705, https://doi.org/10.1002/polb.24576.

[10] M. Herath, J. Epaarachchi, M. Islam, L. Fang, J. Leng, Light activated shape memory polymers and composites: a review, Eur. Polym. J. 136 (2020) 109912, https://doi.org/10.1016/j.eurpolymj.2020.109912.

[11] X. Wang, Y. He, Y. Liu, J. Leng, Advances in shape memory polymers: remote actuation, multi-stimuli control, 4D printing and prospective applications, Mater. Sci. Eng.: R: Rep. 151 (2022) 100702, https://doi.org/10.1016/j.mser.2022.100702.

[12] X. Pang, J. Lv, C. Zhu, L. Qin, Y. Yu, Photodeformable azobenzene-containing liquid crystal polymers and soft actuators, Adv. Mater. 31 (2019) 1904224, https://doi.org/10.1002/adma.201904224.

[13] W. Francis, A. Dunne, C. Delaney, L. Florea, D. Diamond, Spiropyran based hydrogels actuators—walking in the light, Sens Actuators B Chem. 250 (2017) 608–616, https://doi.org/10.1016/j.snb.2017.05.005.

[14] M. Pilz da Cunha, E.A.J. van Thoor, M.G. Debije, D.J. Broer, A.P.H.J. Schenning, Unravelling the photothermal and photomechanical contributions to actuation of azobenzene-doped liquid crystal polymers in air and water, J. Mater. Chem. C Mater. 7 (2019) 13502–13509, https://doi.org/10.1039/C9TC04440J.

[15] J. Lall, H. Zappe, Understanding photomechanical behavior of liquid crystalline-based actuators, Macromol. Mater. Eng. 308 (2023) 2300063, https://doi.org/10.1002/mame.202300063.

[16] Z. Li, X. Zhang, S. Wang, Y. Yang, B. Qin, K. Wang, T. Xie, Y. Wei, Y. Ji, Polydopamine coated shape memory polymer: enabling light triggered shape recovery, light controlled shape reprogramming and surface functionalization, Chem. Sci. 7 (2016) 4741–4747, https://doi.org/10.1039/C6SC00584E.

[17] K. Wang, X.X. Zhu, Two-way reversible shape memory polymers containing polydopamine nanospheres: light actuation, robotic locomotion, and artificial muscles, ACS Biomater. Sci. Eng. 4 (2018) 3099–3106, https://doi.org/10.1021/acsbiomaterials.8b00671.

[18] C.Y. Lo, Y. Zhao, C. Kim, Y. Alsaid, R. Khodambashi, M. Peet, R. Fisher, H. Marvi, S. Berman, D. Aukes, X. He, Highly stretchable self-sensing actuator based on conductive photothermally-responsive hydrogel, Mater. Today 50 (2021) 35–43, https://doi.org/10.1016/j.mattod.2021.05.008.

[19] J. Loomis, B. King, T. Burkhead, P. Xu, N. Bessler, E. Terentjev, B. Panchapakesan, Graphene-nanoplatelet-based photomechanical actuators, Nanotechnology 23 (2012) 045501, https://doi.org/10.1088/0957-4484/23/4/045501.

[20] Y. Bai, J. Zhang, D. Wen, P. Gong, X. Chen, A poly (vinyl butyral)/graphene oxide composite with NIR light-induced shape memory effect and solid-state plasticity, Compos Sci. Technol. 170 (2019) 101–108, https://doi.org/10.1016/j.compscitech.2018.11.039.

[21] Y. Wang, A. Dang, Z. Zhang, R. Yin, Y. Gao, L. Feng, S. Yang, Repeatable and reprogrammable shape morphing from photoresponsive gold nanorod/liquid crystal elastomers, Adv. Mater. 32 (2020) 2004270, https://doi.org/10.1002/adma.202004270.

[22] H. Koerner, G. Price, N.A. Pearce, M. Alexander, R.A. Vaia, Remotely actuated polymer nanocomposites—stress-recovery of carbon-nanotube-filled thermoplastic elastomers, Nat. Mater. 3 (2004) 115–120, https://doi.org/10.1038/nmat1059.

[23] D. Martella, S. Nocentini, D. Nuzhdin, C. Parmeggiani, D.S. Wiersma, Photonic microhand with autonomous action, Adv. Mater. 29 (2017) 1704047, https://doi.org/10.1002/adma.201704047.

[24] M. Pilz da Cunha, H.S. Kandail, J.M.J. den Toonder, A.P.H.J. Schenning, An artificial aquatic polyp that wirelessly attracts, grasps, and releases objects, Proc. Natl. Acad. Sci. 117 (2020) 17571–17577, https://doi.org/10.1073/pnas.2004748117.

[25] M. Pilz da Cunha, S. Ambergen, M.G. Debije, E.F.G.A. Homburg, J.M.J. den Toonder, A.P.H.J. Schenning, A soft transporter robot fueled by light, Adv. Sci. 7 (2020) 1902842, https://doi.org/10.1002/advs.201902842.

[26] H. Zeng, P. Wasylczyk, C. Parmeggiani, D. Martella, M. Burresi, D.S. Wiersma, Light-fueled microscopic walkers, Adv. Mater. 27 (2015) 3883–3887, https://doi.org/10.1002/adma.201501446.

[27] M. Yamada, M. Kondo, J. Mamiya, Y. Yu, M. Kinoshita, C.J. Barrett, T. Ikeda, Photomobile polymer materials: towards light-driven plastic motors, Angew. Chem. Int. Ed. 47 (2008) 4986–4988, https://doi.org/10.1002/anie.200800760.

[28] X. Guo, T. Mao, Z. Wang, P. Cheng, Y. Chen, S. Ma, Z. Zhang, Fabrication of photoresponsive crystalline artificial muscles based on PEGylated covalent organic framework membranes, ACS Cent. Sci. 6 (2020) 787–794, https://doi.org/10.1021/acscentsci.0c00260.

[29] G. Vitale, B. Grandinetti, S. Querceto, D. Martella, C. Tesi, C. Poggesi, E. Cerbai, D. S. Wiersma, C. Parmeggiani, C. Ferrantini, L. Sacconi, Photoresponsive polymer-based biomimetic contractile units as building block for artificial muscles, Macromol. Mater. Eng. 307 (2022) 2200187, https://doi.org/10.1002/mame.202200187.

[30] A.H. Gelebart, D. Jan Mulder, M. Varga, A. Konya, G. Vantomme, E.W. Meijer, R.L. B. Selinger, D.J. Broer, Making waves in a photoactive polymer film, Nature 546 (2017) 632–636, https://doi.org/10.1038/nature22987.

[31] S. Crespi, N.A. Simeth, B. König, Heteroaryl azo dyes as molecular photoswitches, Nat. Rev. Chem. 3 (2019) 133–146, https://doi.org/10.1038/s41570-019-0074-6.

[32] J. Xiong, J. Chen, P.S. Lee, Functional fibers and fabrics for soft robotics, wearables, and human–robot interface, Adv. Mater. 33 (2021) 2002640, https://doi.org/10.1002/adma.202002640.

[33] C. Gotti, A. Sensini, A. Zucchelli, R. Carloni, M.L. Focarete, Hierarchical fibrous structures for muscle-inspired soft-actuators: a review, Appl. Mater. Today 20 (2020) 100772, https://doi.org/10.1016/j.apmt.2020.100772.

[34] G.V. Stoychev, L. Ionov, Actuating fibers: design and applications, ACS Appl. Mater. Interfaces 8 (2016) 24281–24294, https://doi.org/10.1021/acsami.6b07374.

[35] C. Gotti, A. Sensini, G. Fornaia, C. Gualandi, A. Zucchelli, M.L. Focarete, Biomimetic hierarchically arranged nanofibrous structures resembling the architecture and the passive mechanical properties of skeletal muscles: a step forward toward artificial muscle, Front Bioeng. Biotechnol. 8 (2020), https://doi.org/10.3389/fbioe.2020.00767.

[36] A. Sensini, C. Gotti, J. Belcari, A. Zucchelli, M.L. Focarete, C. Gualandi, I. Todaro, A.P. Kao, G. Tozzi, L. Cristofolini, Morphologically bioinspired hierarchical nylon 6,6 electrospun assembly recreating the structure and performance of tendons and ligaments, Med. Eng. Phys. 71 (2019) 79–90, https://doi.org/10.1016/j.medengphy.2019.06.019.

[37] A. Liguori, S. Pandini, C. Rinoldi, N. Zaccheroni, F. Pierini, M.L. Focarete, C. Gualandi, Thermoactive smart electrospun nanofibers, Macromol. Rapid Commun. 43 (2022) 2100694, https://doi.org/10.1002/marc.202100694.

[38] Q. He, Z. Wang, Y. Wang, Z. Wang, C. Li, R. Annapooranan, J. Zeng, R. Chen, S. Cai, Electrospun liquid crystal elastomer microfiber actuator, Sci. Robot 6 (2021) eabi9704, https://doi.org/10.1126/scirobotics.abi9704.

[39] H. Lv, H. Chi, X. Yang, J. Peng, W. Wang, D. Tang, Polydopamine-assisted shape memory of polyurethane nanofibers with light-induced tunable responsiveness and improved cell adhesiveness, Colloids Surf. A Physicochem Eng. Asp. 627 (2021) 127100, https://doi.org/10.1016/j.colsurfa.2021.127100.

[40] X. Wei, L. Chen, Y. Wang, Y. Sun, C. Ma, X. Yang, S. Jiang, D. Duan, An electrospinning anisotropic hydrogel with remotely-controlled photo-responsive deformation and long-range navigation for synergist actuation, Chem. Eng. J. 433 (2022) 134258, https://doi.org/10.1016/j.cej.2021.134258.

[41] K. Paderni, S. Pandini, S. Passera, F. Pilati, M. Toselli, M. Messori, Shape-memory polymer networks from sol–gel cross-linked alkoxysilane-terminated poly (ε-caprolactone), J. Mater. Sci. 47 (2012) 4354–4362, https://doi.org/10.1007/s10853-012-6289-2.

[42] S. Pandini, F. Baldi, K. Paderni, M. Messori, M. Toselli, F. Pilati, A. Gianoncelli, M. Brisotto, E. Bontempi, T. Riccò, One-way and two-way shape memory behaviour of semi-crystalline networks based on sol–gel cross-linked poly (ε-caprolactone), Polymer (Guildf.) 54 (2013) 4253–4265, https://doi.org/10.1016/j.polymer.2013.06.016.

[43] J. García-Amorós, D. Velasco, Recent advances towards azobenzene-based light-driven real-time information-transmitting materials, Beilstein J. Org. Chem. 8 (2012) 1003–1017, https://doi.org/10.3762/bjoc.8.113.

[44] S. Pandini, S. Agnelli, A. Merlettini, F. Chiellini, C. Gualandi, K. Paderni, M. L. Focarete, M. Messori, M. Toselli, Mutifunctional electrospun nonwoven mats with two-way shape memory behavior prepared from sol–gel crosslinked poly (ε-caprolactone), Macromol. Mater. Eng. 302 (2017) 1600519, https://doi.org/10.1002/mame.201600519.

[45] A. Merlettini, S. Pandini, S. Agnelli, C. Gualandi, K. Paderni, M. Messori, M. Toselli, M.L. Focarete, Facile fabrication of shape memory poly(ε-caprolactone) non-woven mat by combining electrospinning and sol–gel reaction, RSC Adv. 6 (2016) 43964–43974, https://doi.org/10.1039/C6RA05490K.

[46] L. Liverani, A. Liguori, P. Zezza, C. Gualandi, M. Toselli, A.R. Boccaccini, M. L. Focarete, Nanocomposite electrospun fibers of poly(ε-caprolactone)/bioactive glass with shape memory properties, Bioact. Mater. 11 (2022) 230–239, https://doi.org/10.1016/j.bioactmat.2021.09.020.

[47] S. Pandini, T. Riccò, A. Borboni, I. Bodini, D. Vetturi, D. Cambiaghi, M. Toselli, K. Paderni, M. Messori, F. Pilati, F. Chiellini, C. Bartoli, Tailored one-way and two-way shape memory capabilities of poly(ε-caprolactone)-based systems for biomedical applications, J. Mater. Eng. Perform. 23 (2014) 2545–2552, https://doi.org/10.1007/s11665-014-1033-5.

[48] A.H. Gelebart, G. Vantomme, E.W. Meijer, D.J. Broer, Mastering the photothermal effect in liquid crystal networks: a general approach for self-sustained mechanical oscillators, Adv. Mater. 29 (2017) 1606712, https://doi.org/10.1002/adma.201606712.

[49] F. Aleotti, A. Nenov, L. Salvigni, M. Bonfanti, M.M. El-Tahawy, A. Giunchi, M. Gentile, C. Spallacci, A. Ventimiglia, G. Cirillo, L. Montali, S. Scurti,

M. Garavelli, I. Conti, Spectral tuning and photoisomerization efficiency in push–pull azobenzenes: designing principles, J. Phys. Chem. A 124 (2020) 9513–9523, https://doi.org/10.1021/acs.jpca.0c08672.
[50] J. Garcia-Amorós, D. Velasco, Understanding the fast thermal isomerisation of azophenols in glassy and liquid-crystalline polymers, Phys. Chem. Chem. Phys. 16 (2014) 3108, https://doi.org/10.1039/c3cp54519a.
[51] T. Chung, A. Romo-Uribe, P.T. Mather, Two-way reversible shape memory in a semicrystalline network, Macromolecules 41 (2008) 184–192, https://doi.org/10.1021/ma071517z.
[52] K. Wang, Y.G. Jia, C. Zhao, X.X. Zhu, Multiple and two-way reversible shape memory polymers: design strategies and applications, Prog. Mater. Sci. 105 (2019) 100572, https://doi.org/10.1016/j.pmatsci.2019.100572.
[53] J. Han, S. Lai, Y.T. Chiu, Two-way multi-shape memory properties of peroxide crosslinked ethylene vinyl-acetate copolymer (EVA)/polycaprolactone (PCL) blends, Polym. Adv. Technol. 29 (2018) 2010–2024, https://doi.org/10.1002/pat.4309.
[54] M. Lahikainen, H. Zeng, A. Priimagi, Reconfigurable photoactuator through synergistic use of photochemical and photothermal effects, Nat. Commun. 9 (2018) 4148, https://doi.org/10.1038/s41467-018-06647-7.
[55] A.P. Murcia, J.M.U. Gomez, J.U. Sommer, L. Ionov, Two-way shape memory polymers: evolution of stress *vs* evolution of elongation, Macromolecules 54 (2021) 5838–5847, https://doi.org/10.1021/acs.macromol.1c00568.
[56] M. Huang, X. Dong, L. Wang, J. Zhao, G. Liu, D. Wang, Two-way shape memory property and its structural origin of cross-linked poly(ε-caprolactone), RSC Adv. 4 (2014) 55483–55494, https://doi.org/10.1039/C4RA09385B.
[57] V. Crescenzi, G. Manzini, G. Calzolari, C. Borri, Thermodynamics of fusion of poly-β-propiolactone and poly-ε-caprolactone. Comparative analysis of the melting of aliphatic polylactone and polyester chains, Eur. Polym. J. 8 (1972) 449–463, https://doi.org/10.1016/0014-3057(72)90109-7.
[58] C.C. Chang, C.M. Huang, Y.H. Chang, C. Kuo, Enhancement of light scattering and photoluminescence in electrospun polymer nanofibers, Opt. Express 18 (2010) A174, https://doi.org/10.1364/OE.18.00A174.
[59] X. Li, J. Zhou, Z. Quan, L. Wang, F. Li, X. Qin, J. Yu, Light scattering tunability of nanofiber membrane for enhancing color yield, Dyes Pigments 193 (2021) 109462, https://doi.org/10.1016/j.dyepig.2021.109462.
[60] S.M. Mirvakili, I.W. Hunter, Artificial muscles: mechanisms, applications, and challenges, Adv. Mater. 30 (2018) 1704407, https://doi.org/10.1002/adma.201704407.
[61] J.D. Madden, Mobile robots: motor challenges and materials solutions, Science 318 (2007) 1094–1097, https://doi.org/10.1126/science.1146351.
[62] Q. Yang, C. Peng, J. Ren, W. Zhao, W. Zheng, C. Zhang, Y. Hu, X.A. Zhang, Near-infrared photoactuator based on shape memory semicrystalline polymers toward light-fueled crane, grasper, and walker, Adv. Opt. Mater. 7 (2019) 1900784, https://doi.org/10.1002/adom.201900784.
[63] H.F. Lu, M. Wang, X.M. Chen, B.P. Lin, H. Yang, Interpenetrating liquid-crystal polyurethane/polyacrylate elastomer with ultrastrong mechanical property, J. Am. Chem. Soc. 141 (2019) 14364–14369, https://doi.org/10.1021/jacs.9b06757.

Michele Zanoni took the Master's Degree in Chemistry in 2021 with full marks. Since then he has worked as a researcher at the University of Bologna's Polymer Science and Biomaterials Group. His research delves into nanofibrous piezoelectric polymeric materials for sensor technology and energy harvesting, alongside shape memory polymers activated by stimuli like light, temperature, and electricity.

Alessio Cremonini obtained his Ph.D. in Chemical Sciences from Bologna University in 2023, defending a Thesis on photoresponsive polymeric materials.

Maurizio Toselli is Associate Professor in Chemistry at University of Bologna since 2002. His present research activity is devoted to the preparation and study of functional and stimuli-responsive materials with particular interest in organic-inorganic hybrid coating and innovative shape memory polymers.

Marco Montalti is Professor of Chemistry at the Department "Giacomo Ciamician" of the University of Bologna in Italy. Activity of his research group is devoted to the development and characterization of biocompatible nanostructures for nanomedicine, energy conversion and environmental remediation.

Daniele Natali obtained his Master in Industrial Chemistry with full marks in 2020. He has work at University of Bologna in collaboration with S.A.C.M.I. industry (2021–2022) and won a fellowship to work at the European Laboratory for Non-Linear Spectroscopy (Florence, Italy, 2021). He is currently a Ph.D. student in Industrial Chemistry at the University of Bologna. His research topics are stimuli-responsive materials, focusing on shape-memory polymers.

Maria Letizia Focarete received her Ph.D. degree from the University of Bologna in 2000. She is currently full professor of Science and Technology of Polymeric Materials at the University of Bologna. Her research interests include polymers for biomedical applications, hydrogels for 3D-bioprinting, innovative bioinspired scaffolds for tissue engineering and drug delivery, bioplastics, stimuli-responsive and functional polymeric materials.

Stefano Masiero received his Ph.D. in Organic Chemistry in 1991 from Bologna University. He is currently Associate Professor of Organic Chemistry at the same University. His research interests are in the field of organized systems and energy conversion.

Chiara Gualandi received her Ph.D. degree in Industrial Chemistry from the University of Bologna in 2010. She is currently Associate Professor at the Chemistry Department "Giacomo Ciamician" (Bologna, Italy). Her research interests focus on stimuli-responsive and functional polymers, including mechano-responsive materials, photo-responsive materials, thermo-reversible polymeric systems and shape-memory polymers.